SHEAR-INSTABILITY IN POSTSTENOTIC ARTERIAL FLOWS

Francois Mallinger, Dimitris Drikakis*
Queen Mary, University of London
Engineering Department,
London E1 4NS, UK
F.Mallinger@qmw.ac.uk, d.drikakis@qmw.ac.uk

ABSTRACT

The paper is concerned with instabilities and transition-to-turbulence in pulsatile flows through a stenosis. Our long term objective is to obtain a better understanding of the flow phenomena associated with diseases such as atherosclerosis and stroke. This can potentially help the development of better diagnostic criteria and clinical detection techniques. Using high-order Godunov-type methods and advanced non-linear multigrid algorithms we have performed three-dimensional simulations of the pulsatile flow through a 75% stenosis and investigate the details of the flow development with particular interest in the poststenotic region. Our simulations reveal the formation of a three-dimensional instability which leads to a strongly disturbed flow extended up to 50-60 radius downstream of the stenosis. This flow behaviour subsequently affects the wall shear stress distribution.

INTRODUCTION

In the context of biofluid dynamics, the computational study of flows through stenoses is motivated by the need to obtain a better understanding of the impact of flow phenomena on diseases such as atherosclerosis and stroke. The flow phenomena occuring in stenotic arteries include asymmetric flow separation, instabilities, laminar-to-turbulent transition and turbulence. These phenomena are also expected to have profound effects on the wall-shear stress distribution. Past experimental studies have shown that in pulsatile flows not only regions of high wall shear-stress are important, but also regions of low wall shear-stress can have important haemodynamic effects due to their rapid variations in space and time (Ku et al., 1985; Caro et al., 1971). A comprehensive review of past experimental and theoretical studies has been presented by Berger and Lou (2000).

*Corresponding author.

Another important issue in stenotic flows concerns medical diagnosis. By analyzing the noise generated by a poststenotic disturbed flow it may be possible to localize artery constriction. Experiments have been performed by Clark (1980) aiming at analyzing turbulence produced by stenosis as well as by Khalifa and Giddens (1981) aiming at relating the level of disturbances of the poststenotic flow to the degree of stenotic obstruction.

Although the above studies have contributed towards a better understanding of stenotic flows, the problem is far from being well understood. To the best of the authors knowledge, a computational study of three-dimensional pulsatile flow, featuring *instabilities, transition and/or turbulence*, through a stenosis, has not yet been presented. Past computational studies are mainly concerned with steady and unsteady axisymmetric flows; for example, we refer the reader to the recent study by Stroud et al. (2000) in which a numerical investigation of the flow in stenotic axisymmetric vessels with different shapes was presented.

In this paper our objectives are i) to study the formation of instabilities and coherent structures in pulsatile flows through a three-dimensional stenosis, and ii) to examine the effects of instability and laminar-to-turbulent transition on the wall shear-stress, velocity and vorticity fields.

PROBLEM DESCRIPTION

The stenosis model considered here is similar to the one used by Khalifa and Giddens (1981). This consists of an axisymmetric stenosis with reduction of 75 % in the cross-sectional area (Fig. 1). The length of the pipe is $2D$ and $70D$ (D is the diameter of the pipe), upstream and downstream of the constriction, respectively. Our grid contains 250,000 cells; this grid size was found to be a good compromise between accuracy and computational cost.

The inlet streamwise velocity $u_i(\mathbf{r},t)$ is defined by a perturbed parabolic profile

$$u_i(\mathbf{r},t) = \left[u_m + u_a sin(\omega t) + f(\mathbf{r},t)\right]\left[1+\left(\frac{|\mathbf{r}|}{R}\right)^2\right],$$

where the inlet centreline velocity is given by the sum of the mean velocity $u_m = 41\,cm/s$ and the sine wave of frequency $\omega = 2\pi$ and amplitude $u_a = 10\,cm/s$ (Fig. 1); $\mathbf{r}$ is the radial vector with origin the centre of the pipe and R is the radius of the pipe. The function $f(\mathbf{r},t)$ is a time-dependent white-noise perturbation with amplitude equal to 20% of the centreline streamwise velocity; similar perturbations are also imposed to the other two velocity components. No-slip boundary conditions are defined on the walls of the pipe. At the outlet, the second-order derivatives of the flow variables are set equal to zero; the present length of the pipe was found sufficient to provide independence of the numerical results from the outlet boundary conditions. The instantaneous Reynolds number, based on the centreline streamwise velocity and the pipe radius, R, has minimum and maxium values of 760 and 1245, respectively. The flow parameters correspond to a pulsatile frequency number (Womersley number) $\alpha = R(\omega/\nu)^{1/2} = 9.87$.

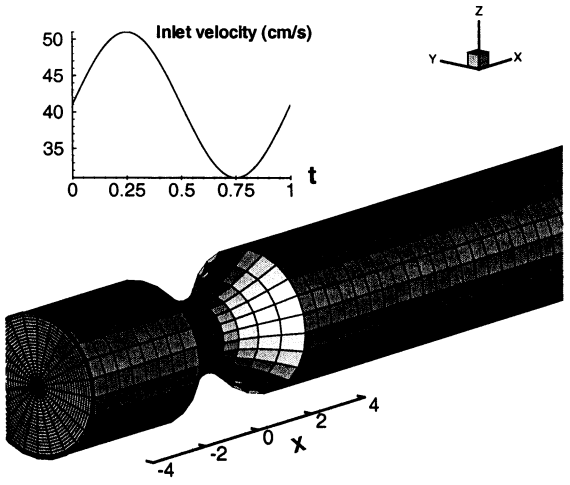

Figure 1: The inlet velocity profile (top) and shape of the stenosis used in the computations (bottom); the unit is the radius of the pipe R. The contriction length is $4R$.

COMPUTATIONAL MODELLING

In our study we have employed the three-dimensional Navier-Stokes equations for an incompressible fluid. Although our computational code can handle both Newtonian and non-Newtonian fluids, here we have assumed the fluid to be Newtonian, a generally valid approximation of the rheological behaviour of blood in the larger blood vessels; additionally, we have considered the arterial wall to be rigid. The above two assumptions are introduced in order to simplify the analysis of our simulations and enable us to develop a gradual understanding of the unstable transitional flow through a stenosis.

Our computational code employs the finite volume approach and curvilinear coordinates. The numerical algorithm is based on high-order Godunov-type schemes (Drikakis, 2001) and a non-linear multigrid method in conjunction with a TVD fourth-order Runge-Kutta scheme for the time integration (Drikakis et al., 1998). The continuity and momentum equations are solved in a coupled fashion via the dual-time stepping/artificial-compressibility approach. The present method allows large time steps to be employed without degrading the stability of the numerical solution. Therefore, 100 time steps per pulsation cycle were found to be sufficient for obtaining the onset and development of the three-dimensional instability. For more details regarding the numerical method, we refer the reader to (Drikakis, 2001; Drikakis et al., 1998).

ONSET OF THE INSTABILITY

Computations were performed for several cycles until the instability has been fully established[1]. The values of the flow variables are not exactly the same across different cycles due to the time-dependence of the flow perturbation at the inlet, as well as due to the transitional nature of the flow. In qualitative terms, however, the flow evolves in a similar fashion across different pulsation cycles after the instability is established.

Fig. 2 shows the isocontours of the streamwise velocity at different cross sections for $t = 0.2$; this time is close to the end of the first acceleration phase of the pulsation cycle. The onset of the instability takes place inside the stenosis region and at $x = 2.5$ (just downstream of the constriction) the instability has already been established; this can be seen as a breaking of the flow symmetry[2] in the velocity contours in the cross-sectional plane (Fig. 2). At $x = 2.5$, the breaking of flow symmetry is associated with the formation of a vortical structure on the upper part of the cross

[1] Nine to eleven cycles were found sufficient for obtaining the onset of the instability as well as its spatial growth.

[2] Symmetry-breaking bifurcations have also been investigated in the past in the context of two-dimensional suddenly expanded flows (Drikakis, 1997).

section. The instability spreads further downstream resulting in additional vortical structures ($x = 7.5$ and $x = 17.5$ in Fig. 2). These structures emerge from the near-wall region, grow further downstream and occupy most of the cross-sectional area. Closer to the stenosis region the breaking of the flow axisymmetry is primarily due to intense streamwise changes of the flow. Further downstream, e.g. at $x = 50.3$, the flow is also affected by circumferential changes resulting in intense swirling motion. This behaviour persists over few radius downstream of the position $x = 50.3$ before the flow turns to be fully axisymmetric again.

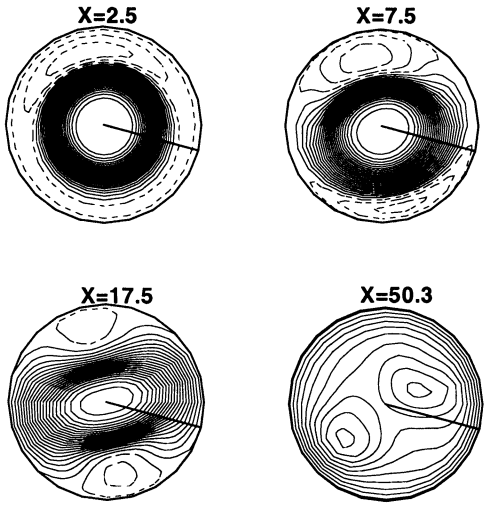

Figure 2: Isocontours of the streamwise velocity at $t = 0.2$, for different cross sections in the streamwise direction.

In relation to the spatial growth of the instability, we identified two poststenotic regions; these can be observed in the isosurfaces of the streamwise velocity at $t = 0.2$ (Fig. 3) and $t = 0.8$ (Fig 5); the corresponding isocontours of the streamwise velocity at $t = 0.8$ and different streamwise positions are shown in Fig. 4. The first region (henceforth labelled "region A") is closer to the constriction and encompasses the fluid jet arising from the stenotic region. In the region A, the instability has already initiated, but it has not broken the coherency of the jet. As second region (henceforth labelled "region B") we identify the region further downstream where large variations of the flowfield occur. In this region, the coherency of the fluid jet cannot be maintained due to the swirling motion of the fluid. As we will demonstrate in the next Section, the region B is associated with large variations of the circumferential shear stress. Although the length of the regions A and B varies across the pulsation cycle, the largest flow variations occur at about 30 to 50 radius downstream of the stenosis. The isocontours in Fig. 4 ($t = 0.8$) show similar effects as for $t = 0.2$, with the only difference being the strength of the instability for all streamwise positions; this is indicated by the extend of the flow asymmetries in the cross sectional planes.

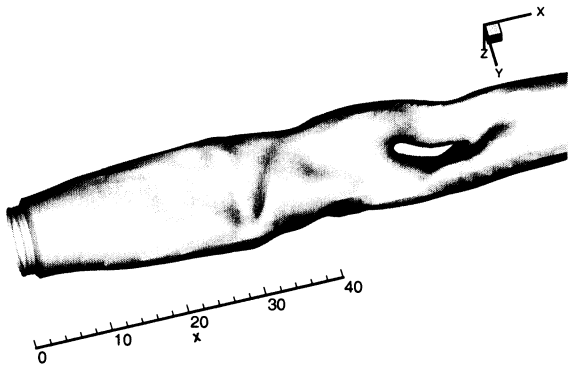

Figure 3: Isosurface $u = 0.92$ of the streamwise velocity at $t = 0.2$.

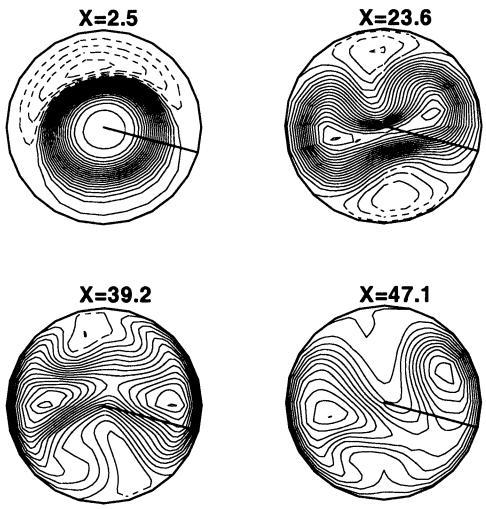

Figure 4: Isocontours of the streamwise velocity at $t = 0.8$, for different cross sections in the streamwise direction.

Fig. 6 shows the streamtraces of the velocity field at different time instants for the cross-section at $x = 30$. Streamtraces in a plane give only a partial picture of the topology of the 3D flow. Nevertheless, this is sufficient to show the changes in the topology of the flow during the pulsation cycle. We observe that the critical points (points of zero velocity) vary in number and location between different time instants (Fig. 6).

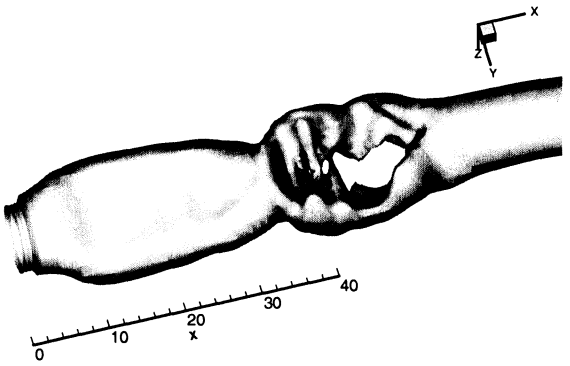

Figure 5: Isosurface $u = 0.92$ of the streamwise velocity at $t = 0.8$.

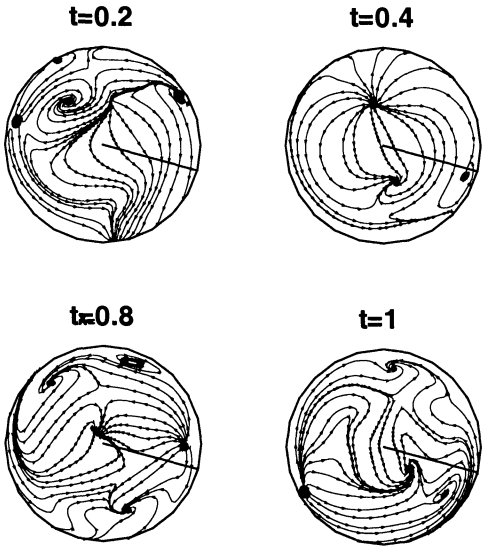

Figure 6: Streamtraces of the velocity field at $x = 30$ and different time instants.

WALL SHEAR STRESS

As mentioned in the introduction, the wall shear-stress is of great importance in physiological flows. Fig. 7 shows isocontours of the longitudinal component, τ_{xn}, of the wall shear-stress at five different time instants; τ_{xn} is calculated by projecting the velocity vector onto a direction tangent to the wall, facing the streamwise direction. Fig. 7 shows that the separated flow region, indicated by negative shear stress, is extended up to 60 radius ($t = 0.8$) downstream of the stenosis. The extend of the separation is reduced at the earlier time instants of the pulsation cycle.

Futher, in the region A we observe elongated structures emerging from the exit of the stenosis. These elongated structures are due to the compression of the fluid jet by the two

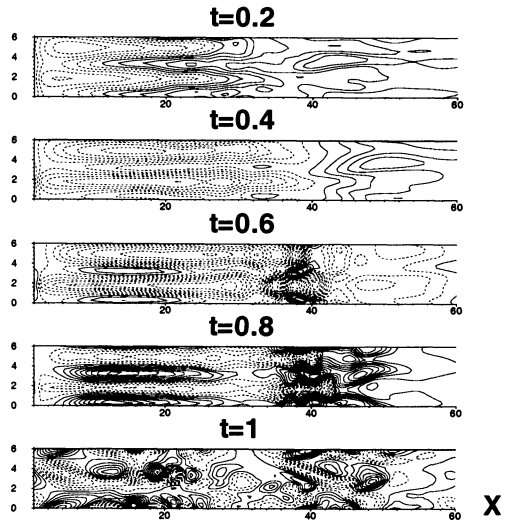

Figure 7: Isocontours of τ_{xn} at different time instants; Dashed and solid lines denote negative and positive stresses, respectively.

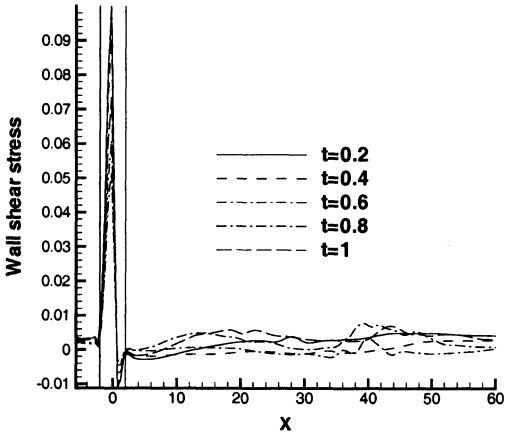

Figure 8: Distribution of maximum τ_{xn} (for each cross section) at five different time instants. The two vertical lines represent the beginning and end of the constriction.

vortical structures observed in the cross sections of the streamwise velocity contours in Figs. 2 and 4. The compression effect also leads to the formation of "bubbles" (Fig. 7 for $t = 0.6 \div 1$) of positive wall shear-stress, inside the regions of negative stresses. Strong mixing of positive and negative stresses occurs between $x = 35$ and $x = 45$. For all time instants the largest values of τ_{xn} appear in the stenotic region (Fig. 8). The peak value occurs at the centre of the stenosis.

In Fig. 9, we have plotted the isocontours of the circumferential component of the shear stress τ_{tn}; the latter is calculated by projecting the velocity vector onto a direction tangent to the wall, orthogonal to the streamwise direction. Similar to τ_{xn}, elongated structures of τ_{tn} also appear close to the constriction region,

but they extend to a smaller area compared to τ_{xn}. Another observation is that the mixing of regions of positive and negative stresses is more evident for τ_{tn} than τ_{xn}. The maximum values of τ_{tn} at each cross section are plotted in Fig. 10. The results show that τ_{tn} is significantly smaller, as expected, than τ_{xn} in the region of the stenosis (see also Fig. 8). On the other hand, large variations of τ_{tn} occur in the region B with the peak value of τ_{tn} occuring at $x = 40$ (Fig. 10). This is in accord with the results discussed in the previous section regarding the bursting of flow coherency and development of swirling motion in the region B.

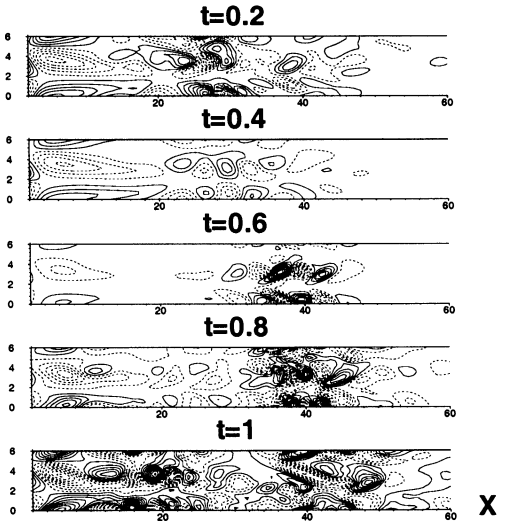

Figure 9: Isocontours of τ_{tn} at different time instants.

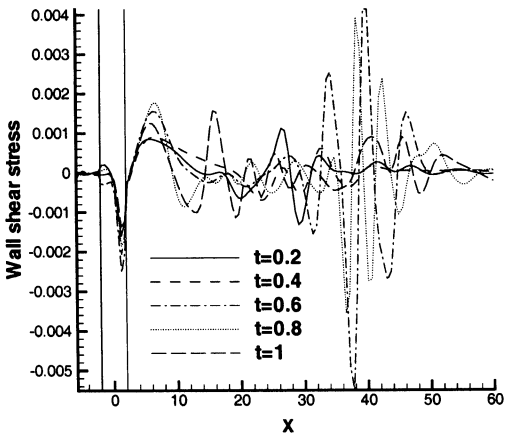

Figure 10: Distribution of maximum τ_{tn} (for each cross section) at five different time instants. The two vertical lines represent the beginning and end of the constriction.

VORTICITY

In this section, we discuss the changes of the vorticity field in the regions A and B. Fig. 11 shows the zero isosurface of the streamwise vorticity, ω_x, at $t = 0.4$. In the region A the surface consists of a superposition of elongated vorticity sheets. Further downstream, these sheets roll up to form cones facing the streamwise direction. The zero isosurface separates volumes of positive (gray) and negative (black) streamwise vorticity (Fig. 12). Elongated "half-ring" like structures, formed by positive and negative vorticity, arise from the exit of the stenosis and terminate at about $x = 21$ (Fig. 12). Further downstream, these structures break up into smaller ones because of the full development of the 3D instability. In the region B, positive and negative vorticity regions alternate both in streamwise and radial directions.

Fig. 13 shows the longitudinal distribution of the maximum (per cross section) value of the vorticity component ω_x at different time instants. The vorticity exhibits large variations in the region B during the deceleration phase of the pulsation. This is in accord with our previous observations that intense swirling of the flow occurs in this region. Moreover, ω_x exhibits a peak value in the stenosis where the onset of instability takes place.

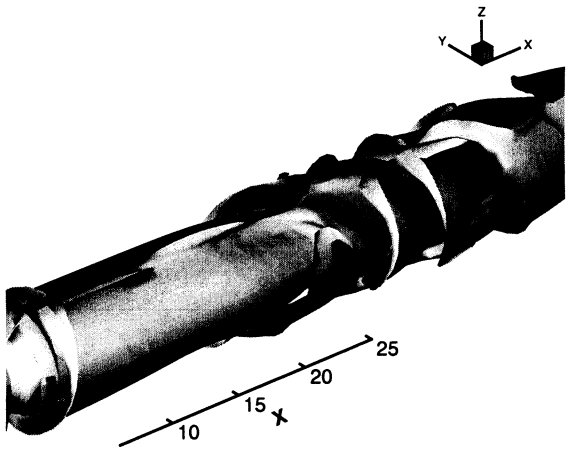

Figure 11: Zero isosurface of the streamwise vorticity ω_x at $t = 0.4$.

CONCLUDING REMARKS

Our numerical simulations of three-dimensional pulsatile flow through a symmetric stenosis revealed the existence of an instability with profound effects on the flow development. Analysis of the velocity, vorticity and shear-stress fields revealed the formation of two poststenotic regions in which significant flow changes occur. In the first region, closer to the constriction, the instability is mainly

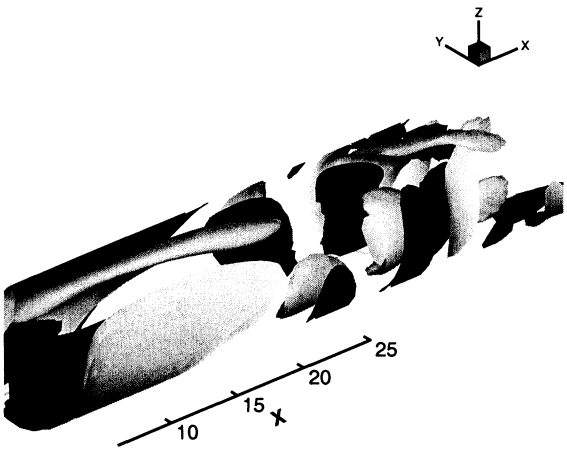

Figure 12: Volumes of positive (gray) and negative (black) streamwise vorticity ω_x at $t = 0.4$.

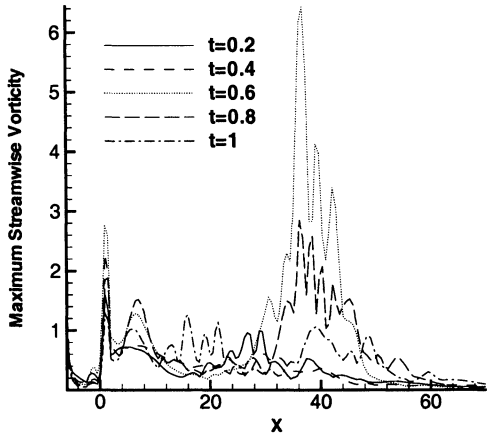

Figure 13: Distribution of the maximum (per cross section) value of the vorticity component ω_x at different time instants.

associated with streamwise flow changes. In this region the instability grows, but it does not lead to decomposition of the coherency of the fluid jet arising from the stenotic region. The second region occurs further downstream and is associated with intense swirling of the flow, breaking of the jet's coherency, increase of the circumferential stress component, as well as large spatial and temporal fluctuations of the stress, velocity and vorticity values. The above conspire to the conclusion that in the second region laminar-to-turbulent transition occurs.

Bearing in mind that rapid variations of the wall shear stress are of paramount importance in the development of vascular diseases, our results suggest that in the diagnostic criteria and detection techniques used in the clinical practice, attention should be given not only to the characteristics of the flow in the stenotic region, but also to the poststenotic region where instability and highly disturbed flow primarily occur. The present results suggest that these regions may extend up to 60 radius downstream of the stenosis.

ACKNOWLEDGEMENTS

The financial support from EPSRC (GR/ L71568) is gratefully acknowledged.

REFERENCES

Berger, S.A., Lou, L-D., 2000, "Flows in stenotic vessels", *Annual Rev. Fluid Mech.*, Vol. 32, pp. 347-382.

Caro, C.G., Fitzgerald, J.M., Schroter, R.C., 1971, "Atheroma and arterial wall shear observations, correlation and proposal of a shear dependent mass transfer mechanism for artherogenesis", *Proc. Royal Soc. London Ser. B*, Vol.17(7), pp. 109-159.

Clark, C., 1980, "The propagation of turbulence produced by a stenosis", *J. Biomechanics*, Vol. 13, pp. 591-604.

Drikakis, D., 1997, "Study of bifurcation flow phenomena in incompressible sudden-expansion flows," *Physics of Fluids*, 9(1), pp. 76-87.

Drikakis, D., Iliev, O., Vassileva, DP., 1998, "A non-linear full multigrid method for the three-dimensional incompressible Navier-Stokes equations", *J. Comput. Physics*, Vol. 146, pp. 301-321.

Drikakis, D., 2001, "Uniformly high-order methods for unsteady incompressible flows," Chapter in the book *Godunov Methods: Theory and Applications*, Kluwer Academic Publishers (ed. E.F. Toro), pp. 263-283.

Khalifa, A.M.A., Giddens, D.P., 1981, "Characterization and evolution of post-stenotic flow disturbances", *J. Biomechanics*, Vol. 14, No. 5, pp. 279-296.

Ku, D.N., Giddens, D.P., Downing, J.M., 1985, "Pulsatile flow and atherosclerosis in the humna carotid bifurcation", *Arteriosclerosis*, Vol. 5(3), pp. 293-302.

Lieber, B. B., Giddens, Don P., 1988, "Apparent stresses in disturbed pulsatile flows", *J. Biomechanics*, Vol. 4, No. 21, pp. 287-298.

Stroud, J.S., Berger, S.A., Saloner, D., 2000, "Influence of stenosis morphology on flow through severely stenotic vessels: implications for plaque rupture", *J. Biomechanics*, Vol. 33, pp. 443-455.